ELSEVIER

Journal of Nuclear Materials 266–269 (1999) 1045–1050

journal of nuclear materials

A CFD onion-skin model for the interpretation of edge experiments

W. Fundamenski *, P.C. Stangeby, J.D. Elder

Institute for Aerospace Studies, University of Toronto, 4925 Dufferin Street, Toronto, Ont., Canada M3H 5T6

Abstract

Earlier onion-skin modelling, O-SM, of divertor edge plasmas, which uses experimental target measurements of I_{sat} and T_e as boundary conditions, has shown good agreement with standard 2-D code solutions, except for detached plasma conditions. The inability to produce stable, detached solutions motivated the development of an improved O-SM solver using standard CFD techniques, which overcame earlier stability problems. A smooth transition between attached and detached regimes has been observed by reducing target T_e with fixed I_{sat}. In the case of strong detachment, typically with T_e below 1 eV, it is found that upstream quantities are highly sensitive on the input target conditions. The solutions show the characteristic detachment profiles both along and across the magnetic field.

Keywords: Divertor plasma; Detachment; 2-D fluid model; SOL modeling

1. Introduction

In standard 2-D CFD (Computational Fluid Dynamics) modelling of tokamak edge plasmas, e.g. EDGE2D, B2, UEDGE, etc., the plasma-fluid equations are solved with flows across the separatrix and cross-field transport coefficients as inputs. In contrast, the Onion-Skin Modelling (O-SM) approach employs target information as input, typically Langmuir probe measurements of $I_{sat.}$ and T_e across the targets. The output in both cases is a 2-D plasma solution for the entire edge region. A comparison of the O-SM approach with the EDGE2D plasma code for low- and high-recycling divertor cases showed good agreement only for attached scenarios [1]; the parabolized formulation employed in the previous O-SM solver turned out to be unstable for detached divertor cases.

The objective of the present work was to develop a CFD solver for O-S Modelling of detached divertor plasmas, to be used for the interpretation of edge impurity and other experimental measurements. The physical basis of the model is discussed both generally, in the context of standard 2-D approaches, and specifically to the work at hand, listing the equations used and assumptions employed. Numerical methods are treated briefly, including a schematic of the computational algorithm. Results for weak and strong detachment are presented, and the performance of the new method assessed.

2. Physical model

2.1. General description

Starting from a set of gyro-averaged kinetic equations, one for each plasma species, in which the distinction between velocities parallel and transverse to the magnetic field is made explicit, $f(x, V_{||}, V_{\perp}, t)$, and taking the three lowest moments leads naturally to the generalised plasma fluid equations [2,3], which can be written in the conservative form as

$$\frac{\partial U}{\partial t} = \nabla_{||} \cdot (F_{||} + G_{||}) + \nabla_{\perp} \cdot (F_{\perp} + G_{\perp}) + Q, \qquad (1)$$

* Corresponding author. Tel.: 1 416 667 7891; fax: 1 416 667 7799; e-mail: wojciech@starfire.utias.utoronto.ca

0022-3115/99/$ – see front matter
PII: S0022-3115(98)00852-6

where U represents the plasma fluid variables, F the convective fluxes, G the diffusive fluxes expressed in terms of transport coefficients along and across the magnetic field, $(D_{||}, D_{\perp}, \eta_{||}, \eta_{\perp}, \chi_{||}, \chi_{\perp})$ and Q the source terms including the interaction between plasma and neutral species. These are the equations, usually written in primitive variables $(n, u_{||}, p_e, p_i)$, which are most often employed in edge plasma modelling. Assuming toroidal symmetry, $\partial/\partial\phi = 0$, and neglecting drift terms, they can be written in terms of poloidal co-ordinates (r, s), where s is the distance along a field line projected onto the poloidal plane and r the cross field distance, and solved numerically on a poloidal domain consisting of the scrape-off-layer and the private-flux region, hence bounded by the separatrix and the target,

$$\frac{\partial U(r,s)}{\partial t} = \frac{1}{J_s}\frac{\partial}{\partial s}[J_s(F_s + G_s)] + \frac{1}{J_r}\frac{\partial}{\partial r}[J_r(F_r + G_r)] + Q[U(r,s)], \quad (2)$$

where F_s, F_r, G_s, G_r, are the F an G fluxes in those directions, and J_s, Jr the Jacobian elements of the transformation, $J_r = 1$, $J_s = B/B_{\mathrm{pol}}$, i.e. $s_{||} = J_s s, F_{||} = J_s F_s$, $F_{\perp} = J_r F_r$, etc.

The standard 2-D CFD approach requires knowledge of the cross-field coefficients ($D_{\perp}$, $\eta_{\perp}$, $\chi_{\perp}$) which are anomalous and therefore not known, a priori. A further problem in using such codes for interpretation of edge experiments is the fact that the principal experimental measurements (I_{sat}, T_e) at the targets, are difficult to impose directly as boundary conditions, without over-constraining the system of equations. Finding the closest match to near target measurements can require lengthy parameter searches [4].

The above considerations, along with the fact that plasma transport along the magnetic field lines is much stronger than across them ($u_{||} \gg u_{\perp}, \chi_{||} \gg \chi_{\perp}$), motivated the development of a solution method for the plasma fluid equations generally termed Onion-Skin Modelling (O-SM). The method consists in imposing the mass and energy fluxes at the targets as boundary conditions and replacing the cross field terms by simple source terms $Q_{\perp}$, normalized to satisfy mass, momentum and power balance on each computational flux tube,

$$\frac{\partial U(r,s)}{\partial t} = \frac{\partial}{\partial s_{||}}(F_{||} + G_{||}) + Q_{\perp}(Q, U_0) + Q\big[U(r, s_{||})\big], \quad (3)$$

where $s_{||}$ is the distance along a field line and $U_0(r) = U(r, 0)$ represents the target conditions. The removal of the radial derivative allows the equations to be solved in 1-D along each flux tube; by treating each flux tube in this way, a 2-D plasma solution $U(r,s) = U(r, s_{||}B_{\mathrm{pol}}/B)$ is constructed. It is important to note that although each flux tube is solved independently of the others with given sources Q, these sources depend on the transport of neutral particles and hence on the entire 2-D plasma profile, i.e. $Q = Q[U(r, s)]$. When $U(Q)$ and $Q(U)$ are repeatedly iterated in this way, the 2-D nature of the solution is made apparent.

Previous comparisons between O-SM and 2-D codes have shown close agreement between the two methods for low and high recycling cases. However, stable detached solutions could not be obtained using the O-SM approach [1]. Since then, an improved O-SM method has been developed specifically to capture detached solutions; the details of the physical model used in this most recent attempt are presented below, while a summary of the numerical methods employed is given in the following section.

2.2. Specific description

The plasma fluid equations can be simplified further for single ion species and very strong energy coupling between ions and electrons ($T_e \approx T_i \approx T$),

$$\frac{\partial U}{\partial t} = \frac{\partial}{\partial s_{||}}(F_{||} + G_{||}) + Q_{\perp} + Q_{\mathrm{MC}}, \quad (4)$$

$$U = \begin{pmatrix} \rho \\ \rho u \\ \rho E \end{pmatrix}, \quad F_{||} = \begin{pmatrix} \rho u \\ \rho + \rho u^2 \\ u(\frac{5}{2}p + \frac{1}{2}\rho u)^2 \end{pmatrix},$$

$$G_{||} = \begin{pmatrix} o \\ \delta p \\ q_{||} + \delta p \end{pmatrix}, \quad (5)$$

$$Q_{\mathrm{MC}} = \begin{pmatrix} m(Q_{\mathrm{iz}} - Q_{\mathrm{rec}} \\ mV_H Q_{\mathrm{iz}} - muQ_{\mathrm{rec}} - m(u - V_H)Q_{\mathrm{CX}} \\ \frac{1}{2}mV_H^2 Q_{\mathrm{iz}} - \frac{1}{2}mu^2 Q_{\mathrm{rec}} - Q_{\mathrm{qe}} + Q_{\mathrm{qi}} - Q\mathrm{z} \end{pmatrix}, \quad (6)$$

where $\rho = mn$, $u = u_{||}$, $p = n(T_e + T_i) = 2nT$, and $\rho E = 1.5p + 0.5\ \rho u^2$. The case of arbitrary ion–electron energy coupling will be treated in work still to be published [5], however we expect strong T_e and T_i coupling in the dense, cold, near target region. The diffusive fluxes $q_{||}$ and δp are calculated using Braginskii parallel transport coefficients for ions and electrons $(\eta_{||}^i, \chi_{||}^i, \chi_{|}^e)$ with a flux limited ion viscosity. In the work presented here, the volumetric sources of ionization Q_{iz}, recombination Q_{rec}, ion–neutral charge exchange Q_{CX}, and electron energy loss due to ionization, dissociation and excitation Q_{qe} were calculated using a Monte Carlo (MC) neutral transport code, NIMBUS [6]; ion energy term was set to zero, $Q_{\mathrm{qi}} = 0$, as was the neutral velocity along B, $V_H = 0$, while the effect of impurity cooling was estimated by $Q_Z = f_{Z,\mathrm{qe}} Q_{\mathrm{qe}}$, with $f_{Z,\mathrm{qe}} = 1$. These assumptions were made for the sake of simplicity rather than accuracy; the effect of other Q_{qi}, V_H and Q_Z models will be explored in future work [5]. The $V_H = 0$ assumption corresponds to an upper limit on the amount

of momentum loss due to CX collisions. The cross-field sources $Q_\perp(s)$ were updated according to specified profiles along B, and normalized such that the net sources $Q = Q_{\rm MC} + Q_\perp$ integrated along a flux tube were equal to the sum of the parallel target fluxes, i.e. $\langle Q^{(j)}\rangle = 2(F_{\|(j)} + G_{\|(j)})0,\ j = 1,2,3$, for symmetrical target conditions, which were assured by symmetrizing the sources. The cross-field particle source $Q_\perp^{(1)}$ was assumed proportional to density, while for the power source $Q_\perp^{(3)}$ a symmetric step function profile, $\Theta_{(s)} = \Theta(s_{\max} - s)$, was used with no power input for the first 20% of the flux tube, roughly the X-point location; $s_{\max}$ is the target to target distance along the flux tube in the poloidal plane. A cross-field momentum source $Q_\perp^{(2)}$ was set equal to zero, since in the present study sources were symmetrized around the mid-point between the targets. Combining the above, we can write

$$Q_\perp = \begin{pmatrix} C_1 n(s) \\ 0 \\ C_3\Theta(s - 0.2s_{\max}) \end{pmatrix}; \quad \begin{array}{l} C_1\langle n(s)\rangle + \langle Q_{\rm MC}^{(1)}\rangle \\ \quad = 2m\Gamma_o \\ C_3\langle\Theta(s - 0.2s_{\max})\rangle, \\ \langle Q_{\rm MC}^{(3)}\rangle = 2q_o, \end{array} \tag{7}$$

where Γ_0 and q_0 are the target particle and power fluxes parallel to B for each flux tube, and $\langle ...\rangle$ denote flux tube integrals. Two further boundary conditions were imposed at the target: the velocity was limited by the target sound speed according to the Bohm criterion, $M_0 = u_\|/\sqrt{(2T/m)} \geqslant 1$, and the power flux was related to the target temperature by the sheath heat transmission coefficients for ions and electrons,

$$q_0 = (\gamma_{\rm e} + \gamma_{\rm i})T_0\Gamma_0,\ \gamma_{\rm e} = 5.0,\ \gamma_{\rm i} = 2.5 + M_0^2.$$

3. Numerical methods

In the previous work [1], an inviscid form of the plasma equations was parabolized and solved using a Runge–Kutta quadrature along each flux tube. The inability of the parabolized scheme to capture plasma detachment plus the desire to include viscous effects indicated the need for a fully elliptic solution method. A 1-D solver was written using standard CFD techniques [5,7]: (a) conservative formulation, (b) variable, non-staggered grid adaptation minimising ΔU, (c) implicit time update with local time stepping, including both convective and viscous Jacobian terms, (d) block-tridiagonal matrix inversion, and (e) extrapolated boundary conditions. Typical time for reconvergence to within an error of 1% and a maximum residual of 10^{-4} was roughly 5 CPU s per flux tube ($\sim$1 min for the whole SOL) on an IBM RS6000 3AT machine.

The sources Q $(r,\ s)$ for the plasma equations were calculated using NIMBUS; the background plasma Q $(r,\ s)$ was transferred from the finer, along-B CFD grid onto the standard poloidal grid generated to match the magnetic field profile of an experimental discharge. The calculated sources $Q_{\rm MC}(r,s)$ were then relaxed with the previous sources, $Q = a_{\rm relax}Q_{\rm new} + (1 - a_{\rm relax})Q_{\rm old}$, $a_{\rm relax} < 0.1$ and mapped back onto the CFD grid. The relaxation assured gradual evolution and counteracted statistical error present in MC results with a finite number of particle histories.

The iterative computational cycle can be represented as a triple process: (a) CFD solution for the plasma $U(r,s)$ based on most recent sources, (b) MC solution for sources $Q_{\rm MC}(r,s)$ based on the new plasma and a relaxation with the previous sources, (c) a parametric update of cross field sources based on $Q_{\rm MC}$ and target boundary conditions U_0, which gives the new sources $Q = Q_{\rm MC} + Q_\perp$;

$$\begin{array}{ccc} U[Q] & \rightarrow & Q_{\rm MC}[U] \\ \uparrow & & \downarrow \\ Q = Q_{\rm MC} + Q_\perp & \leftarrow & Q_\perp(Q_{\rm MC}, U_0) \end{array}. \tag{8}$$

The above computational cycle can be converged in two ways: (a) by specifying the input power into each ring $P_{\rm in}(r)$ and the target particle flux $\Gamma_0(r)$, and allowing the target temperature $T_0(r)$ to change according to the radiated power $P_{\rm MC}(r)$, or (b) by specifiying $T_0(r)$ and $\Gamma_0(r)$, which gives the target power flux $q_0 = (\gamma_{\rm e} + \gamma_{\rm i})T_0\Gamma_0$, and adjusting $P_{\rm in}(r)$ according to $P_{\rm MC}(r)$. Referring to the former as the predictive mode, and the latter as the interpretive mode, we can summarise them as,

$$\begin{array}{l} \text{Predictive mode: } \{\Gamma_0(r), P_{\rm in}(r)\} \rightarrow \{U(r,s), T_0(r)\} \\ \text{Interpretive mode: } \{\Gamma_0, T_0(r)\} \rightarrow \{U(r,s), P_{\rm in}(r)\} \end{array},$$

Two comments should be made about the uniqueness and stability of the interpretive mode solutions. Firstly, it was observed that, if a stable solution could be found for a given set of target conditions $\{\Gamma_0(r), T_0(r)\}$ then that solution appeared to be unique. If the solution was not stable, it was concluded that the target conditions were physically inadmissible, e.g. the extreme case of $(\Gamma_0(r) > 0,\ T_0(r) = q_0(r) = 0$; in that case, $T_0(r)$ was increased until the solution was stabilised. Secondly, it was found that for strongly detached solutions, typically with sub-eV target temperatures, small changes in $T_0(r)$ resulted in significant changes in the upstream plasma $U(r,\ s)$. In practice, since target temperature measurements can not be performed to such high accuracy, it makes more sense when trying to identify an appropriate solution to match a given experiment, to do so on the basis of some upstream quantity, such as the midpoint separatrix value of density, temperature or pressure. In the present work, we have selected the total radiated power from the scrape-off-layer, $P_{\rm SOL} = \Sigma_r P_{\rm MC}(r)$, as such a constraint.

4. Results

Using the method outlined above, self-consistent plasma solutions in the interpretive mode were obtained for a variety of target conditions. Since O-SM solutions for medium and high recycling JET discharges were reported previously [1], it will merely be noted that the new method does not significantly alter solutions in those regimes. Furthermore, since the primary objective of this work was the modelling of detached plasmas, only detached solutions will be presented. The magnetic geometry used in all the cases reported corresponds to a JET ohmic discharge with a MARK-I divertor configuration, Fig. 1.

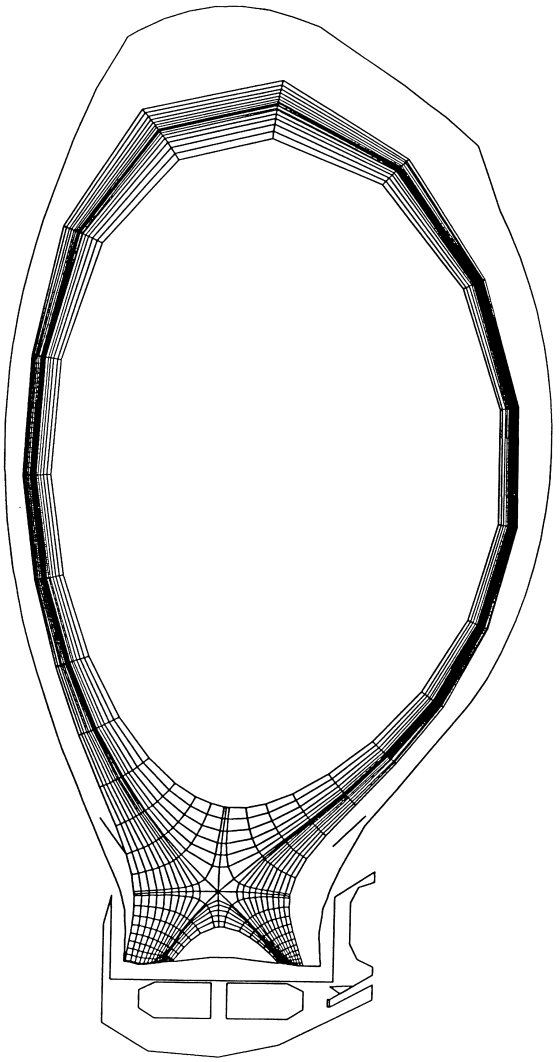

Fig. 1. Standard poloidal grid used by NIMBUS; generated for the magnetic geometry of a JET ohmic discharge with a MARK-I divertor configuration with horizontal targets.

It was observed that starting from an attached solution, as the target temperature T_0 was reduced for a constant Γ_0, eventually a density peak was formed near the target on each flux tube, and its location moved progressively further away from the target, demonstrating a smooth transition between the attached and detached regimes. A similar transition was observed in the predictive mode by decreasing the input power P_{in} for fixed Γ_0, which lead to a gradual detachment of the plasma from the target. Both processes were fully reversible.

4.1. Weak detachment

We first examine the case of a weakly detached plasma obtained with spatially uniform target profiles of $T_0(r)$ and $\Gamma_0(r)$ ($T_0 = 1.0$ eV, $\Gamma_0 = 10^{23}$ m^{-2}s^{-1}, and $M_0 = 1.0$ were used to calculate q_0, which was imposed as a boundary condition). The solution for this case is presented in terms of poloidal profiles parallel and perpendicular to the magnetic field, Fig. 2 Fig. 3. Referring to Fig. 2, we note a region of cold, dense, fast flowing and highly collisional plasma in the vicinity of the target, all of which are characteristic of detachment; although some recombination is present, $\langle Q_{\text{rec}}/Q_{\text{iz}}\rangle \sim 2\%$ on the separatrix flux tube, nearly all momentum loss is due to ion–neutral CX collisions, $\langle Q_{\text{CX}}/Q_{\text{rec}}\rangle \gg 1$. The radial profiles show gradual decay of $P_{\text{in}}(r), T(r)$ and $n(r)$, despite uniform target conditions. As mentioned earlier, the neutral source terms $Q_{\text{MC}}(r,s)$ are responsible for this radial variation: it is clearly not introduced (directly) by the target (boundary) conditions since these are radially constant.

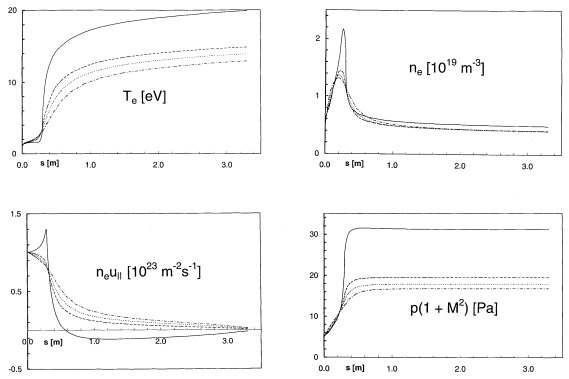

Fig. 2. Weak detachment. Profiles along B, as a function of the poloidal distance s (m), from the inner target, $s = 0$, to the midpoint, $s = 3.3$ m, of temperature, $T_e = T_i = T$, density n_e, parallel plasma flow $n_e u_{||}$ and total pressure $2\, n_e T + n_e m u_{||}^2 = p\,(1 + M^2)$, on four plasma rings. Refer to Fig. 1 for 2-D geometry. Solid line: separatrix ring, $r\# = 8$; dashed line: $r\# = 10$; dotted line: $r\# = 12$; mixed line: $r\# = 14$.

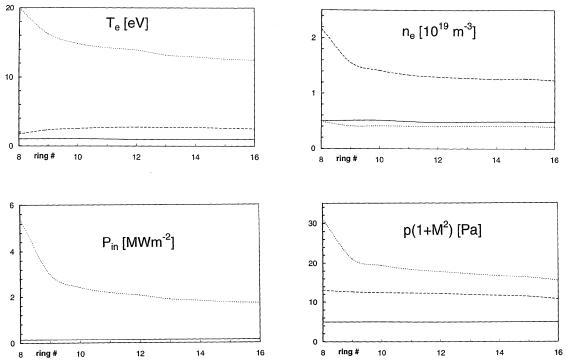

Fig. 3. Weak detachment. Profiles across B, as a function of the ring number, of temperature T_e, density n_e, input power P_{in} and total pressure $2\ n_eT + n_em u_{||}^2 = p\ (1 + M^2)$, at three poloidal locations. Refer to Fig. 1 for 2-D geometry. Solid line: inner target, $s = 0$; dashed line: location of density peak, $s \approx 0.25$ m; dotted line: midpoint, $s = 3.3$ m.

4.2. Strong detachment

In the second case, likewise for uniform target profiles, the target temperature T_0 was reduced by a half, to 0.5 eV, while Γ_0 was kept constant, see Figs. 4 and 5. The stronger detachment is indicated by a flat $T(s)$ profile on all flux tubes, a density $n(s)$ peaking somewhat further away from the target, and very strong momentum loss. As discussed in Section 3, the strong sensitivity of upstream values, such as $n_{max}(s)$ and p_{max}/p_0, on the specified target conditions makes it advantageous to select the desired solution based on an added upstream constraint; in this case, a solution was chosen by requiring that $P_{SOL} = 0.25$ MW. The reason for this sensitivity may be linked to the important role played by recombination below 1 eV, e.g. on the separatrix flux tube $\langle Q_{rec}/Q_{iz}\rangle \sim 1$. Despite significant recombination, it was found that most of the momentum loss was still caused by CX collisions, $\langle Q_{CX}/Q_{rec}\rangle \gg 1$.

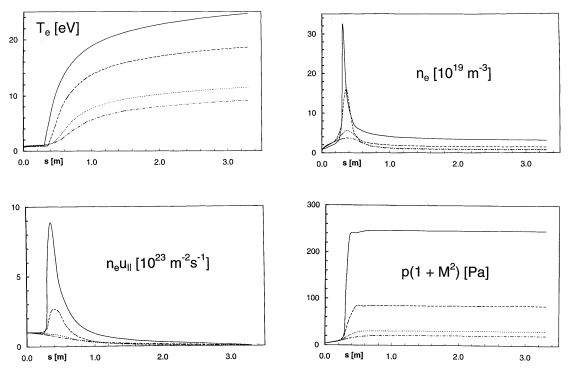

Fig. 4. Strong detachment. Same format as Fig. 2 only for the case of strong detachment.

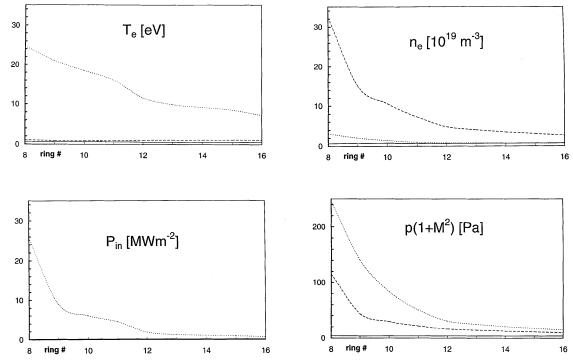

Fig. 5. Strong detachment. Same format as Fig. 3 only for the case of strong detachment.

Comparing Figs. 3 and 5, we note that radial gradients become more pronounced as detachment progresses, in other words, that the flux tube closest to the separatrix begins to detach first. One explanation for this may be offered by the fact, that the distance along the field line near the X-point is larger for the separatrix flux tube due to the weaker poloidal B-field and $s_{||} = (B/B_{pol})s$; this makes the near X-point cells more opaque with respect to momentum loss for ions travelling along that flux tube, enhancing detachment. The tendency of input power to decay radially in strong detachment was confirmed by a case, not presented here, in which the target $T_0(r)$ and $\Gamma_0(r)$ were specified according to a Gaussian profile which peaked away from the separatrix; as before $P_{in}(r)$ fell monotonically in the radial direction, even though the target power actually rose away from the separatrix.

5. Conclusions

The new O-SM solver appears to have overcome the previously encountered stability problems in treating detached divertor solutions. Smooth transition between attached and detached regimes was observed in both the predictive, $\{P_{in}(r), \Gamma_0(r)\}$ specified, and interpretive, $\{T_0(r), \Gamma_0(r)\}$ specified, modes of convergence. Using the latter mode, a unique 2-D edge plasma $U(r,s)$ and input power profile P_{in} (r) can be obtained from the target conditions alone. In strongly detached cases, the plasma solution was found to be highly sensitive to target T_e; thus, in the absence of precise target temperature measurements, some upstream quantity, such as the separatrix density, pressure, or total radiated power, provides a more useful constraint when the aim is to identify a converged solution $U(r, s)$ which best matches given experimental data. The obtained detached solutions show radially decaying upstream power profiles, for both uniform and peaked target conditions, and a region of cold, dense, fast flowing, and highly collisional plasma characteristic of detachment; it was found that

nearly all of the pressure loss was caused by CX collisions, $\langle Q_{CX}/Q_{rec}\rangle \gg 1$, irrespective of the level of recombination, which was small in the case of weak detachment, $\langle Q_{rec}/Q_{iz}\rangle < 1$, but significant for strong detachment, $\langle Q_{rec}/Q_{iz}\rangle \sim 1$. It appears that even though recombination clearly reinforces plasma detachment, it does not do so directly by removing momentum, but rather by a synergetic mechanism involving both recombination and ion–neutral friction.

Despite certain simplifying assumptions in the physical model, which will be removed in the future work, and the sensitivity of strongly detached solutions on the target conditions, which can be circumvented by imposing some upstream constraint, we suggest that detached plasma experiments may be interpreted using the O-SM method described.

References

[1] P.C. Stangeby, J.D. Elder, W. Fundamenski et al., J. Nucl. Mater. 241–243 (1997) 358.
[2] S.I. Braginskii, in: M.A. Leontovich (Ed.), Reviews of Plasma Physics, vol. 1, Consultants Bureau, New York, 1965, p. 205.
[3] E. Zawaideh, N.S. Kim, F. Najmabadi, Phys. Fluids 31 (1988) 3280.
[4] A. Loarte, J. Nucl. Mater. 241–243 (1997) 118–134.
[5] W. Fundamenski, PhD thesis, to be published.
[6] E. Cupini, A. De Matteis, R. Simonini, NET Report, EUR XII (1984) 324/9.
[7] C. Hirsch, Numerical Computation of Internal and External Flows, Wiley, New York, 1990.